J. Fluid Mech. (2023), *vol*. 969, A5, doi:10.1017/jfm.2023.551

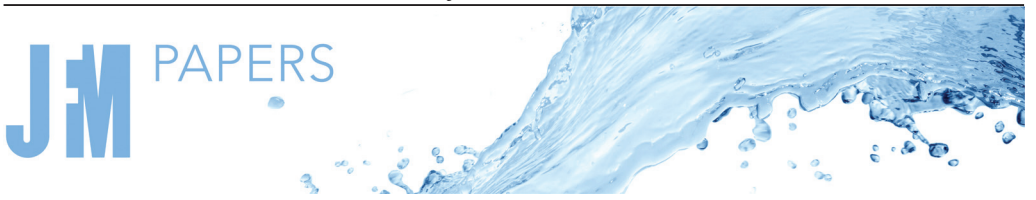

Exact solutions for submerged von Kármán point vortex streets cotravelling with a wave on a linear shear current

Jack S. Keeler[1],† **and Darren G. Crowdy**[2]

[1]School of Mathematics, University of East Anglia, Norwich NR4 7TJ, UK

[2]Department of Mathematics, Imperial College London, 180 Queen's Gate, London SW7 2AZ, UK

(Received 24 February 2023; revised 29 June 2023; accepted 4 July 2023)

New exact solutions are presented to the problem of steadily travelling water waves with vorticity wherein a submerged von Kármán point vortex street cotravels with a wave on a linear shear current. Surface tension and gravity are ignored. The work generalizes an earlier study by Crowdy & Nelson (*Phys. Fluids*, vol. 22, 2010, 096601) who found analytical solutions for a single point vortex row cotravelling with a water wave in a linear shear current. The main theoretical tool is the Schwarz function of the wave, and the work builds on a novel framework set out recently by Crowdy (*J. Fluid Mech.*, vol. 954, 2022, A47). Conformal mapping theory is used to construct Schwarz functions with the requisite properties and to parametrize the waveform. A two-parameter family of solutions is found by solving a pair of nonlinear algebraic equations. This system of equations has intriguing properties: indeed, it is degenerate, which radically reduces the number of possible solutions, although the space of physically admissible equilibria is still found to be rich and diverse. For inline vortex streets, where the two vortex rows are aligned vertically, there is generally a single physically admissible solution. However, for staggered streets, where the two vortex rows are offset horizontally, certain parameter regimes produce multiple solutions. An important outcome of the work is that while only degenerate von Kármán point vortex streets can exist in an unbounded simple shear current, a broad array of such equilibria is possible in a shear current beneath a cotravelling wave on a free surface.

Key words: vortex interactions, general fluid mechanics

† Email address for correspondence: jack.keeler@uea.ac.uk

1. Introduction

In the study of two-dimensional water waves, it is common to assume that the flow is irrotational and to study the effects of gravity or capillarity, or both. There is growing interest, however, in the theory of water waves with vorticity where finite-amplitude steadily travelling waves can exist even without either of these physical effects (Benjamin 1962; Simmen & Saffman 1985; Teles da Silva & Peregrine 1988; Pullin & Grimshaw 1988; Vanden-Broeck 1994, 1996; Sha & Vanden-Broeck 1995; Constantin & Strauss 2004; Groves & Wahlén 2007; Groves & Wahlén 2008; Ehrnström 2008; Wahlén 2009; Hur & Dyachenko 2019*a*,*b*; Hur & Vanden-Broeck 2020; Hur & Wheeler 2020). A recent review article (Haziot *et al.* 2022) gives an overview of some of the literature on water waves with vorticity. When adding vorticity to the water wave problem, there is a choice on the form of the vorticity distribution, and it has traditionally been taken to be uniform: Tsao (1959) and Benjamin (1962) performed early weakly nonlinear analyses of this case. Simmen & Saffman (1985) studied it numerically for gravity waves in deep water, work extended by Teles da Silva & Peregrine (1988) to the finite depth scenario. In the infinite depth case, one supposes that at large distances from the interface, the flow is a linear shear current. By now, much other numerical work has been done for constant-vorticity water waves using a variety of formulations (Vanden-Broeck 1994, 1996; Sha & Vanden-Broeck 1995; Hur & Dyachenko 2019*a*,*b*; Hur & Vanden-Broeck 2020; Hur & Wheeler 2020).

Another vortex model that has been studied in the context of water waves is the point vortex. Early work on the rigorous existence theory, when gravity is present but weak, and when the vorticity is modelled as a point vortex, was carried out by Filippov (1961) and Ter-Krikorov (1958). Shatah, Walsh & Cheng (2013) have proved the existence of steadily travelling two-dimensional capillary–gravity water waves with compactly supported vorticity, including the case where the vorticity is in the form of point vortices. Varholm (2016) constructed solitary solutions for capillary–gravity waves with a submerged point vortex. Le (2019) looked at solitary waves carrying a submerged finite dipole in deep water.

Recently, one of the authors (Crowdy 2022) has introduced a novel theoretical framework for understanding water waves with uniform vorticity, in the absence of gravity or surface tension, and possibly also punctuated by rows of cotravelling point vortices. The mathematical tool used in this framework is the notion of a Schwarz function of a wave. Earlier, Crowdy & Nelson (2010) used Schwarz functions in the context of a water wave problem involving a linear shear current, and the recent work of Crowdy (2022) shows how that study fits into a broader framework.

To explain the Schwarz function of a wave, consider first a flat wave profile $y = 0$, say, in a Cartesian (x, y) plane. Using the complex variable $z = x + \mathrm{i}y$, clearly

$$\bar{z} = z \quad \text{on } y = 0. \tag{1.1}$$

A key observation is that the right-hand side of (1.1) is an analytic function of z having the feature that it can be analytically continued off the line $y = 0$. For a more general wave profile, ∂D say, given by an analytic curve that is periodic in the x direction, the Schwarz function of ∂D can be defined as the function $S(z)$, analytic in a strip containing the wave profile, satisfying the conditions

$$\bar{z} = S(z) \quad \text{on } \partial D, \tag{1.2}$$

with

$$S(z) \to z + \mathrm{i}\Lambda + O(1/z) \quad \text{as } y \to -\infty,\ \Lambda \in \mathbb{R}. \tag{1.3}$$

The Schwarz function of the flat profile (1.1) corresponds to the special case $S(z) = z$ with $\Lambda = 0$.

Schwarz functions are defined most commonly for closed analytic curves, and much is known about their properties and applications (Davis 1974). As shown by Crowdy (2022), it turns out that the generalized notion of the Schwarz function $S(z)$ of a wave profile can be used to express the two-dimensional velocity field (u, v) associated with steadily travelling waves with constant vorticity ω_0, and allowing also for submerged cotravelling periodic rows of point vortices, in the complex variable form

$$u - \mathrm{i}v = -\frac{\mathrm{i}\omega_0}{2}\,\bar{z} + q\sqrt{S'(z)} + \frac{\mathrm{i}\omega_0}{2}\,S(z), \tag{1.4}$$

where (u, v) refers to the velocity field in the cotravelling frame of reference with speed U_f, say. The constant q represents the speed of the fluid on the interface itself; from Bernoulli's condition, this surface speed must be constant if both gravity and surface tension are ignored, and if the region above the fluid region is at constant pressure. Condition (1.3) means that as $y \to -\infty$,

$$u - \mathrm{i}v = \frac{\mathrm{i}\omega_0}{2}\,(z - \bar{z} + \mathrm{i}\Lambda) + q = -\omega_0 y + \left(q - \frac{\Lambda\omega_0}{2}\right), \tag{1.5}$$

so the wave speed is related to the other parameters via

$$U_f = \frac{\Lambda\omega_0}{2} - q. \tag{1.6}$$

In view of the general expression (1.4), three cases arise naturally (Crowdy 2022, pp. 6–7):

(i) case 1: $\omega_0 \neq 0$, $q = 0$, uniform vorticity, zero velocity at the free surface;
(ii) case 2: $\omega_0 = 0$, $q \neq 0$, irrotational flow, non-zero velocity at the free surface;
(iii) case 3: $\omega_0 \neq 0$, $q \neq 0$, uniform vorticity and non-zero velocity at the free surface.

In each case, only special classes of wave profiles will correspond to physically admissible steadily travelling equilibria, and this means only special choices of $S(z)$ are allowed in the expression (1.4). Crowdy (2022) shows how to use conformal mapping theory to find admissible Schwarz functions and, consequently, to construct new analytical solutions to the problem of steadily travelling water waves with vorticity when the distribution is uniform, possibly with superposed point vortices. Other singularity types can easily be admitted too.

Using similar conformal mapping techniques, the aforementioned study of Crowdy & Nelson (2010) found exact solutions for travelling waves on a deep-water linear shear current having constant vorticity and with a single submerged cotravelling point vortex row. Their techniques were borrowed from an earlier study of Crowdy (1999), who posed that streamfunctions taking the form of so-called modified Schwarz potentials can provide equilibrium vortical solutions of the incompressible two-dimensional Euler equations. These have the form

$$\psi(z, \bar{z}) = -\frac{\omega_0}{4}\left[z\bar{z} - \int^z S(z')\,\mathrm{d}z' - \overline{\int^z S(z')\,\mathrm{d}z'}\right], \tag{1.7}$$

for which a simple calculation, with $u = \partial\psi/\partial y$, $v = -\partial\psi/\partial x$, leads to

$$u - \mathrm{i}v = 2\mathrm{i}\,\frac{\partial\psi}{\partial z} = -\frac{\mathrm{i}\omega_0}{2}\,(\bar{z} - S(z)), \tag{1.8}$$

which coincides with (1.4) once the case 1 choice of $q = 0$ is made. It is in this way that the solutions of Crowdy & Nelson (2010) can now be viewed as the most basic water wave solutions falling within the case 1 category of solutions.

In fact, the framework of Crowdy (2022) provides a theoretical unification of three (until now, apparently unrelated) contributions in the water wave literature: those of Crowdy & Nelson (2010), Crowdy & Roenby (2014) and Hur & Wheeler (2020) which, respectively, are now understood as the most basic water wave solutions falling within cases 1, 2 and 3. Interested readers are referred to Crowdy (2022) for a more detailed explanation of these developments.

For present purposes, it is enough to point out that after describing the general framework, Crowdy (2022) focused on producing a range of new solutions falling within the case 2 category. Among these are solutions describing two submerged vortex rows, also known as von Kármán vortex streets, cotravelling with a free surface wave but where the flow was otherwise irrotational; the earlier work of Crowdy & Roenby (2014) had found steady waves cotravelling with a single submerged point vortex row. The purpose of the present paper is to present the 'case 1 analogues' of those new solutions involving two vortex rows: here, we present analytical solutions for submerged von Kármán vortex streets (i.e. two vortex rows) cotravelling in a linear shear current beneath a free surface wave, thereby generalizing the work of Crowdy & Nelson (2010), who focused on a single cotravelling vortex row.

The paper is set out as follows. In § 2, the background on steady equilibria falling within case 1 of the solution taxonomy of Crowdy (2022) is given. Section 3 then describes the classical von Kármán vortex streets in unbounded irrotational flow, and examines whether those equilibria can be generalized to exist in a background simple shear. In § 4, the problem of two submerged vortex rows, or a vortex street, in a linear shear current is formulated. It is shown that finding equilibria within the case 1 category can be reduced to the study of two algebraic equations whose solution structure is discussed in detail in § 5. A characterization of the physically admissible solutions is surveyed in § 6. The paper closes with a discussion of the results in § 7.

2. Case 1 category of solutions

Once the expression (1.4) for the complex velocity field has been derived in terms of the Schwarz function $S(z)$ of the wave profile, the case 1 category of solutions follows simply by taking $q = 0$, which means that the form of the complex velocity field reduces to (1.8), as explained above. This is the generalized viewpoint espoused by Crowdy (2022). However, because the present paper focuses on only case 1 solutions, it is possible to defer to the earlier work of Crowdy & Nelson (2010) and offer a more direct formulation in this case.

A vortex patch is the name given to a region of uniform vorticity (Saffman 1992); an unbounded fluid region of constant vorticity below some wave profile can therefore be viewed as a vortex patch of infinite extent. For any steadily travelling wave on the boundary of a vortex patch, there is a kinematic condition that the vortex jump at the patch boundary in a cotravelling frame of reference must be a streamline. An additional dynamical condition at the vortex jump says that the velocity fields must be continuous there; this turns out to ensure the continuity of the fluid pressure (Saffman 1992).

Suppose now that a streamfunction for a steadily travelling equilibrium over a semi-infinite linear shear layer is given, in a cotravelling frame, by (1.7). It is checked

readily that the free surface is a streamline since, on the vortex jump where $\bar{z} = S(z)$,

$$\mathrm{d}\psi = \frac{\partial\psi}{\partial z}\,\mathrm{d}z + \frac{\partial\psi}{\partial\bar{z}}\,\mathrm{d}\bar{z} = -\frac{\omega_0}{4}\left[(\bar{z} - S(z))\,\mathrm{d}z + \left(z - \overline{S(z)}\right)\mathrm{d}\bar{z}\right] = 0. \tag{2.1}$$

Moreover, since from (1.8) $u - \mathrm{i}v = 0$ on the vortex jump, it is continuous with the vanishing velocity in the upper constant pressure phase. The streamfunction (1.7) therefore appears to furnish a relative equilibrium of the two-dimensional Euler equations even before any choice of $S(z)$ is made, because both the kinematic and dynamic boundary conditions at the vortex jump are satisfied.

The catch is that generic Schwarz functions $S(z)$ have singularities in the region corresponding to the fluid, and as such, only certain choices of $S(z)$ will be admissible physically. Even then, if $S(z)$ has a physically admissible singularity – such as a simple pole with a real residue that corresponds to a point vortex – then there are additional dynamical constraints that any such point vortex is also in equilibrium with respect to the global configuration. While all these constraints might appear, at first sight, to render it unlikely that equilibrium streamfunctions within this class exist, many such solutions have now been found. In the radial geometry most relevant when studying finite-area vortices, such equilibrium solutions have been identified by Crowdy (1999, 2002*a*,*b*) and Crowdy & Marshall (2004, 2005). For the water wave geometry, the aforementioned work of Crowdy & Nelson (2010) provides such solutions; that study focussed on a single submerged point vortex row cotravelling with a wave on the vortex jump on a semi-finite shear layer. The aim of the present paper is to extend the latter class of water wave solutions to the case where a submerged von Kármán vortex street – that is, a pair of vortex rows, either symmetric ('inline') or asymmetric ('staggered') (Acheson 1990; Saffman 1992) – cotravels with a wave on the vortex jump.

3. The classical von Kármán vortex streets

Since the aim here is to study solutions in which vortex streets resembling those studied by von Kármán are cotravelling with a wave in a linear shear current, it is appropriate to review the theory of von Kármán vortex streets, without any background shear, in an unbounded irrotational flow.

The complex potential, $w(z)$ say, for a single periodic point vortex row comprising vortices all having circulation Γ and with period c, is well-known (Acheson 1990; Saffman 1992) to be

$$w(z) = -\frac{\mathrm{i}\Gamma}{2\pi}\log\sin\left(\frac{\pi z}{c}\right), \tag{3.1}$$

where one of the vortices has been placed at the origin. Apart from the point vortices, the flow is otherwise irrotational. The associated complex velocity field is

$$u - \mathrm{i}v = \frac{\mathrm{d}w}{\mathrm{d}z} = -\frac{\mathrm{i}\Gamma}{2c}\cot\left(\frac{\pi z}{c}\right) \to \mp\frac{\Gamma}{2c} \quad \text{as } y \to \pm\infty. \tag{3.2}$$

Far from the vortex row, the fluid velocity is uniform in the x direction but in opposite directions above and below.

A staggered, or asymmetric, von Kármán vortex street is made up of two such point vortex rows, one with vortices of circulation Γ_u above another row with vortices of circulation Γ_l offset by half a period; in the classical setting, $\Gamma_l = -\Gamma_u$, for reasons to

be seen shortly. Such a street, with period $c = 2\pi$, therefore has complex potential

$$-\frac{\mathrm{i}\Gamma_u}{2\pi}\log\sin\left(\frac{z+\mathrm{i}}{2}\right)-\frac{\mathrm{i}\Gamma_l}{2\pi}\log\sin\left(\frac{z-\pi+\mathrm{i}(1+\lambda)}{2}\right), \tag{3.3}$$

where we have now placed one of the vortices in the row having circulation Γ_u at $z = -\mathrm{i}$, and one of the vortices in the row having circulation Γ_l at $z = \pi - \mathrm{i}(1+\lambda)$; this is for ease of comparison with solutions found later. The parameter λ is the aspect ratio of the street (Acheson 1990; Saffman 1992). The associated complex velocity field is

$$u - \mathrm{i}v = -\frac{\mathrm{i}\Gamma_u}{4\pi}\cot\left(\frac{z+\mathrm{i}}{2}\right)-\frac{\mathrm{i}\Gamma_l}{4\pi}\cot\left(\frac{z-\pi+\mathrm{i}(1+\lambda)}{2}\right). \tag{3.4}$$

Since both cotangent functions tend to $\mp\mathrm{i}$ as $y \to \pm\infty$, it is clear that the velocity induced far away from this street will vanish provided that $\Gamma_u = -\Gamma_l := \Gamma$. It is then easy to show, using the usual rules for the velocity of a free point vortex, that the vortex street moves steadily in the x direction, with velocity

$$\frac{\Gamma}{4\pi}\tanh\left(\frac{\lambda}{2}\right). \tag{3.5}$$

It is natural to ask whether such a relative equilibrium can also exist if placed in a simple shear flow, $(-y, 0)$ say. There is no complex potential in this case, but the associated complex velocity field is

$$u - \mathrm{i}v = -y - \frac{\mathrm{i}\Gamma}{4\pi}\cot\left(\frac{z+\mathrm{i}}{2}\right)+\frac{\mathrm{i}\Gamma}{4\pi}\cot\left(\frac{z-\pi+\mathrm{i}(1+\lambda)}{2}\right), \tag{3.6}$$

where the same relationship $\Gamma_u = -\Gamma_l := \Gamma$ is again necessary to ensure that there is no uniform flow component in the far field. Suppose that we assume the existence of a steadily translating equilibrium moving in the x direction with speed U. Then the condition for equilibrium at $y = -1$, or $z = -\mathrm{i}$, is

$$U_{stag} = 1 + \frac{\Gamma}{4\pi}\tanh\left(\frac{\lambda}{2}\right), \tag{3.7}$$

while the condition at $y = -(1+\lambda)$, or $z = -\mathrm{i}(1+\lambda)$, is

$$U_{stag} = 1 + \lambda + \frac{\Gamma}{4\pi}\tanh\left(\frac{\lambda}{2}\right). \tag{3.8}$$

It is clear that (3.7) and (3.8) can be consistent only if $\lambda = 0$, corresponding to a degenerate case, with zero aspect ratio, comprising a periodic row of vortices of alternating circulation spaced apart by π.

A similar conclusion is reached for the inline (also known as unstaggered, or symmetric) von Kármán vortex streets. In this case, provided that $\lambda \neq 0$ (because otherwise the two point vortex rows will sit directly atop each other and cancel each other out), the analogues of the two conditions (3.7) and (3.8) are

$$U_{inline} = 1 + \frac{\Gamma}{4\pi}\coth\left(\frac{\lambda}{2}\right) \tag{3.9}$$

and

$$U_{inline} = 1 + \lambda + \frac{\Gamma}{4\pi}\coth\left(\frac{\lambda}{2}\right). \tag{3.10}$$

Since $\lambda = 0$ is the only consistent solution of both (3.9) and (3.10), and because this value corresponds to the two vortices cancelling each other out, the conclusion is that there is no

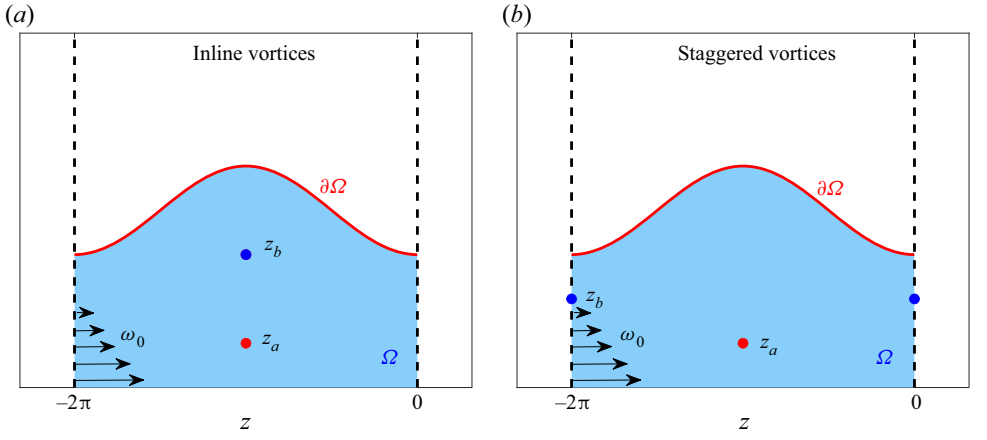

Figure 1. The physical plane for (*a*) inline and (*b*) staggered vortices. The positions of the vortices are denoted z_a and z_b, and the domain is 2π-periodic.

equilibrium for an inline, or symmetric, von Kármán vortex street in an unbounded simple shear current.

These simple calculations reveal that no classical von Kármán vortex street equilibria survive when placed in an unbounded simple shear. Interestingly, however, in what follows we are able to show that equilibria resembling von Kármán vortex streets do survive when the point vortices are cotravelling with a free surface wave in a simple shear current.

4. Von Kármán vortex streets cotravelling with a wave in a linear shear current

The physical situations of interest for the remainder of this paper are illustrated in figures 1(*a*,*b*), which show inline configurations and staggered configurations in a single period window of the complex z plane, respectively. The fluid domain in this 2π-period window is denoted by Ω; it is unbounded as $y \to -\infty$, but bounded above by a free surface, denoted by $\partial\Omega$. As $y \to -\infty$, the flow tends to a linear shear of the form $(-y, 0)$ upon using the dimensionalization $\omega_0 = 1$; this simply sets a time scale for the flow. It is assumed that there are two point vortices in the fluid in each 2π-period window (although more vortices can be added; see the discussion in the previous section). For inline configurations, both are located in the middle of the period window; for the staggered configuration, the vortices are offset by half a period in the x direction (we note that changing the horizontal offsets of the stagger of the two vortices simply changes the length of the period window). Since steadily travelling equilibria with speed U_f in the positive x direction are sought, it is natural to move to a cotravelling frame of reference where, as $y \to -\infty$, the flow is steady and tends to a linear shear of the form $(-y - U_f, 0)$. In this frame of reference, the wave profile is fixed, as are the locations of any submerged point vortices. This means, according to the usual equations of motion of a free point vortex (Acheson 1990; Saffman 1992), that the non-singular component of the velocity field at each point vortex must vanish.

Following the formulation in Crowdy & Nelson (2010), who allowed for a single point vortex per period, or a single submerged vortex row, the extension to two point vortices per period, or two submerged vortex rows, requires consideration of a generalized conformal

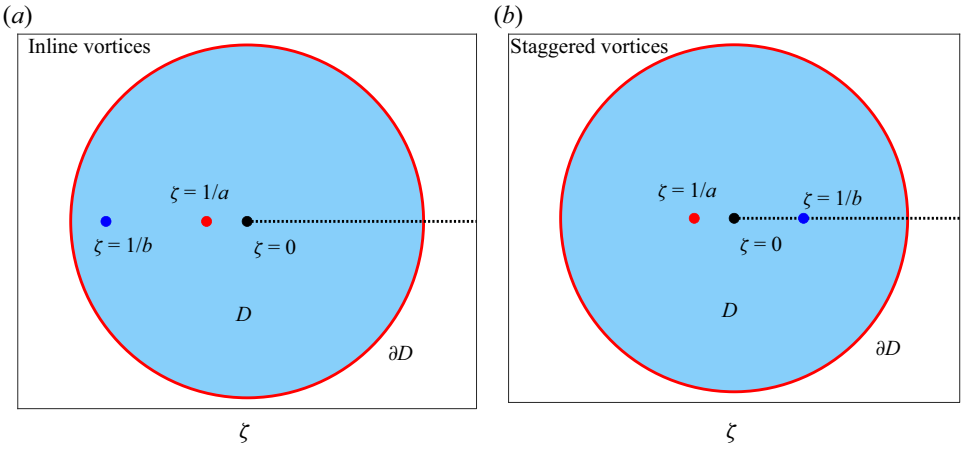

Figure 2. The ζ plane for (a) inline and (b) staggered vortices. The branch cut is shown as a dotted line. The singularities of $\boldsymbol{u}$ are at $\zeta = 1/a$ and $\zeta = 1/b$ (cf. (4.4)) and correspond to the positions of the vortices in the ζ plane.

map of the form

$$z = Z(\zeta) = \mathrm{i}\left[\log\zeta + \frac{A}{\zeta - a} + \frac{B}{\zeta - b}\right] + d, \tag{4.1}$$

where $a, b, A, B \in \mathbb{R}$ and $d \in \mathrm{i}\mathbb{R}$ are parameters to be determined. This mapping transplants a unit disc, in a parametric ζ plane, to the period window Ω in the z plane. Let the interior of the unit disc be denoted by D, and its unit circle boundary by ∂D, as shown in figure 2(a,b) for the inline and staggered cases, respectively. It is necessary that $|a|, |b| > 1$ to ensure that there are no poles of z in D; this is because the conformal mapping must be an analytic function mapping the cut disc in a one-to-one fashion to a period window. The only allowed singularity inside the disc is therefore the logarithmic singularity at $\zeta = 0$ mapping to $y \to -\infty$ and required by the periodic nature of the image domain. The two sides of a logarithmic branch cut between $\zeta = 0, \infty$ are transplanted to the two sides of the period window Ω. The boundary ∂D is transplanted to the free surface $\partial\Omega$ in the physical plane.

To see how (4.1) produces the two point vortices per period, note that the Schwarz function can be written, as a function of ζ, as

$$S(z) = \bar{z} = \overline{Z(\zeta)} = \bar{Z}(1/\zeta) = \mathrm{i}\left[\log\zeta - \frac{A\zeta}{1 - a\zeta} - \frac{B\zeta}{1 - b\zeta}\right] + \bar{d}, \tag{4.2}$$

where we have used the fact that $\bar{\zeta} = 1/\zeta$ on ∂D, and hence on $\partial\Omega$. Since this function has the same logarithmic singularity as $Z(\zeta)$ at $\zeta = 0$, it is easy to check that this function satisfies the far-field condition (1.3). The Schwarz function $S(z)$ has simple poles at $\zeta = 1/a, 1/b$, which are inside D and therefore correspond to simple poles of $S(z)$ at

$$\left.\begin{aligned} z_a &= Z(1/a) = \mathrm{i}\left[\log(a^{-1}) + \frac{Aa}{1 - a^2} + \frac{Ba}{1 - ab}\right] + d, \\ z_b &= Z(1/b) = \mathrm{i}\left[\log(b^{-1}) + \frac{Bb}{1 - b^2} + \frac{Ab}{1 - ab}\right] + d \end{aligned}\right\} \tag{4.3}$$

which are inside Ω. The two parameters a and b will be viewed as free parameters. It then turns out that for equilibrium, $A = A(a, b)$, $B = B(a, b)$ and $d = d(a, b)$ must be

determined as functions of these two parameters. To see this, notice that the complex velocity field (1.8) can be written as a function of ζ as

$$u - \mathrm{i}v = -\frac{\mathrm{i}\omega_0}{2}\,[\bar{z} - S(z)] = -\frac{\omega_0}{2}\left[\log|\zeta|^2 + \frac{A}{\bar{\zeta} - a} + \frac{B}{\bar{\zeta} - b} - \frac{A\zeta}{1 - \zeta a} - \frac{B\zeta}{1 - \zeta b}\right]. \tag{4.4}$$

To find the condition that the point vortex at $\zeta = 1/a$ is in equilibrium, it is useful to rewrite the velocity field as

$$u - \mathrm{i}v = -\frac{\omega_0}{2}\left[\log|\zeta|^2 + \frac{A}{\bar{\zeta} - a} + \frac{B}{\bar{\zeta} - b} + \frac{A}{a} + \frac{A}{a^2}\,\frac{1}{(\zeta - 1/a)} + \frac{B\zeta}{1 - \zeta b}\right], \tag{4.5}$$

and then make use of the fact that near $\zeta = 1/a$,

$$\frac{1}{\zeta - 1/a} = \frac{Z'(1/a)}{z - z_a} + \frac{Z''(1/a)}{2Z'(1/a)} + O(z - z_a). \tag{4.6}$$

It follows that near $z = z_a$,

$$u - \mathrm{i}v = -\frac{\omega_0}{2}\left[\frac{A}{a^2}\,\frac{Z'(1/a)}{z - z_a} + S_a + O(z - z_a)\right], \tag{4.7}$$

where

$$S_a = \log(1/a^2) + \frac{Aa}{1 - a^2} + \frac{Ba}{1 - ab} + \frac{A}{a} + \frac{A}{a^2}\,\frac{Z''(1/a)}{2Z'(1/a)} + \frac{B}{b - a}. \tag{4.8}$$

Thus a point vortex of circulation Γ_a at $z = z_a = Z(1/a)$, where

$$-\frac{\mathrm{i}\Gamma_a}{2\pi} = -\frac{A\omega_0\,Z'(1/a)}{2a^2}, \tag{4.9}$$

will be in equilibrium provided that $S_a = 0$. This is the usual equilibrium condition for a free point vortex. By exactly the same reasoning, the point vortex of circulation Γ_b at $z = z_b = Z(1/b)$, where

$$-\frac{\mathrm{i}\Gamma_b}{2\pi} = -\frac{B\omega_0 Z'(1/b)}{2b^2} \tag{4.10}$$

will be in equilibrium provided that $S_b = 0$, where

$$S_b = \log(1/b^2) + \frac{Ab}{1 - b^2} + \frac{Bb}{1 - b^2} + \frac{B}{b} + \frac{B}{b^2}\,\frac{Z''(1/b)}{2Z'(1/b)} + \frac{A}{a - b}. \tag{4.11}$$

The two equilibrium conditions can be rewritten as

$$\left.\begin{aligned} 2a^2\left[\log(1/a^2) + \frac{A}{a(1 - a^2)} + \frac{B(1 - a^2)}{(1 - ab)(b - a)}\right]Z'(1/a) + A\,Z''(1/a) = 0, \\ 2b^2\left[\log(1/b^2) + \frac{A(1 - b^2)}{(1 - ab)(a - b)} + \frac{B}{b(1 - b^2)}\right]Z'(1/b) + B\,Z''(1/b) = 0. \end{aligned}\right\} \tag{4.12}$$

The algebraic form of these equations is

$$\left.\begin{aligned} \lambda_1 A^2 + \lambda_2 B^2 + \lambda_3 AB + \lambda_4 A + \lambda_5 B + \lambda_6 = 0, \\ \mu_1 A^2 + \mu_2 B^2 + \mu_3 AB + \mu_4 A + \mu_5 B + \mu_6 = 0, \end{aligned}\right\} \tag{4.13}$$

where the coefficients $\{\lambda_j, \mu_j \mid j = 1, \ldots, 6\}$ are given as explicit functions of a and b in Appendix A. These equations will be viewed as determining A and B as functions of

a and b, i.e. $A = A(a, b)$, $B = B(a, b)$. Since it determines the possible equilibria, the solution structure of (4.13) is discussed in detail in the next section, not least because it is found to have intriguing and unexpected features. We also note that this framework can be generalized easily to n vortices per period window, which will result in n nonlinear equations similar to (4.13) to solve; but we leave a detailed discussion of this until § 7.

It only remains to fix d. But we are free to set the location of the vortex at z_a so, following Crowdy & Nelson (2010), we set $z_a = -\pi - \mathrm{i}$, i.e. unit distance below $y = 0$ in the middle of the period window. This determines d. An alternative choice is to pick d so that the mean level of the wave profile is specified, but then we would lose control of the position of one of the vortices.

5. The solution structure of (4.13) for A and B

The possibility of finding equilibria has been reduced to determining A and B from the algebraic system (4.13). For a single vortex, the equivalent single equation can be manipulated easily into a closed-form expression that gives A as a straightforward function of a (Crowdy & Nelson 2010). In the present two-vortex case, the analysis is more involved, but as will be discussed here, it shares some interesting and surprising features. Due to the complicated nature of the coefficients λ_i, μ_i, although an analytical solution is possible in principle, it is too cumbersome to gain insight.

One would expect from the general algebraic structure in (4.13), and using Bézout's theorem (Bézout 1779), that, accounting for multiplicity of roots, there will be four pairs of solutions (the number of solutions is the product of the highest power in each equation). Indeed, the solutions (A, B) represent the intersection of two conic sections.

However, by working through the algebra (see Appendix A), surprisingly, it turns out that $\lambda_1 \equiv 0$ and $\mu_2 \equiv 0$ – a result not predictable *a priori*. Therefore $\Delta = \lambda_3^2 - 4\lambda_1\lambda_2 > 0$, thus the two conics are both hyperbolae. One can easily eliminate A, say, from the equations in (4.13) to leave a quartic equation for B, which has four roots, as predicted, with closed-form expressions. Remarkably, again working through the algebra, it turns out that the coefficient of B^4 is zero, namely,

$$\mu_1\lambda_2^2 - \mu_3\lambda_2\lambda_3 \equiv 0. \tag{5.1}$$

This degeneracy implies that (4.13) has only three roots: either one real and two complex, or three real. (We note that this does not contradict Bézout's theorem as the extra root can be accounted for by the intersection of the two hyperbolae at infinity.)

It should be emphasized that a similar phenomenon occurs in the single-vortex analysis of Crowdy & Nelson (2010): a single equation for A is, at first glance, a quadratic equation, but the coefficient of the leading quadratic term is identically zero, resulting in a one-parameter family of solutions (Crowdy & Nelson 2010). More will be said on this observation in § 7.

It is useful to understand this degenerate case by exploring the geometry of the curves defined in (4.13). Examining the large (A, B) behaviour in (4.13), we find that

$$B \sim 0, \quad \lambda_2 B + \lambda_3 A \sim 0, \tag{5.2a,b}$$

$$A \sim 0, \quad \mu_3 B + \mu_1 A \sim 0. \tag{5.3a,b}$$

The asymptotes corresponding to $A \sim 0$ and $B \sim 0$ are vertical and horizontal lines in the (A, B) plane, respectively, and the gradients of the non-trivial asymptotes are $-\lambda_2/\lambda_3$ and $-\mu_3/\mu_1$, respectively. We find that $-\lambda_2/\lambda_3 = -\mu_3/\mu_1 \equiv (1 - b^2)/(a^2 - 1)$, thus

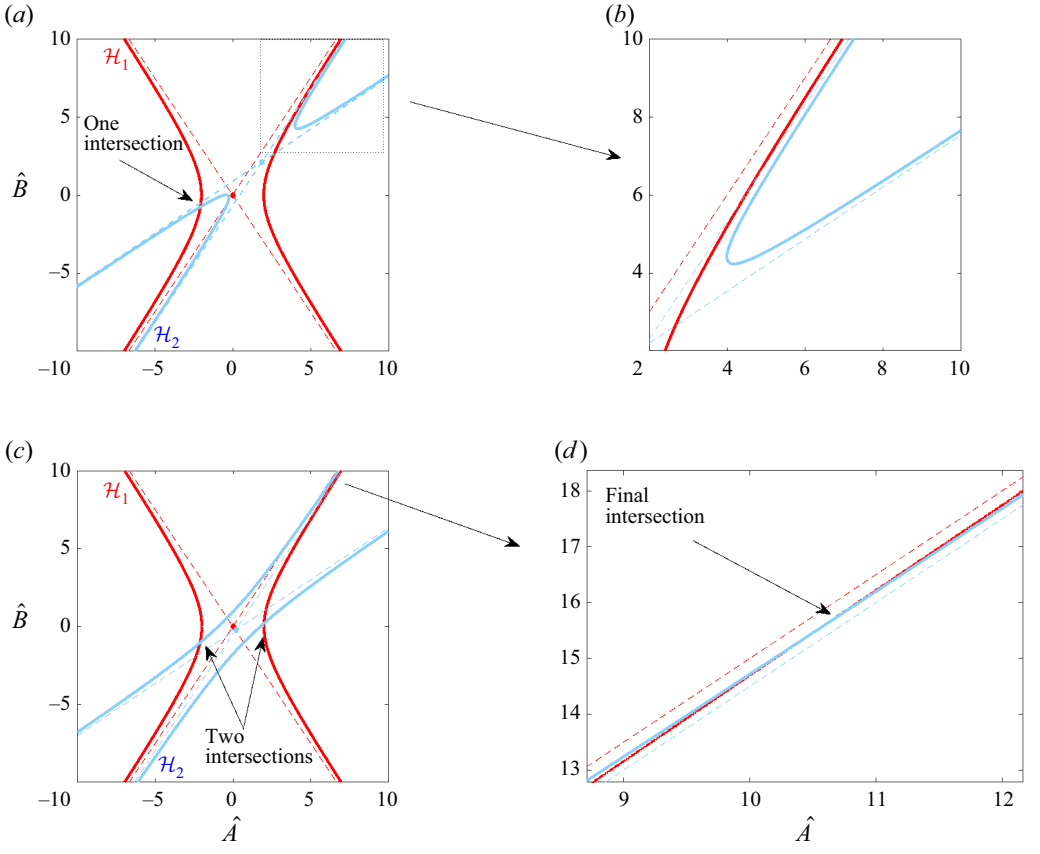

Figure 3. (*a*) Two hyperbolae with the properties described in (5.5) that intersect at one point. (*b*) A zoomed-in image of the rectangular area in (*a*) showing that no further intersection is possible. (*c*) Two hyperbolae with the properties described in (5.5) that intersect at three points. (*d*) A zoomed-in image near to where the third intersection occurs.

the asymptotes are parallel. The problem thus reduces to finding the intersection of two hyperbolae, $\mathcal{H}_1$ and $\mathcal{H}_2$, with the two properties:

$$\text{(1)}\quad \text{one asymptote of } \mathcal{H}_1 \text{ is perpendicular to } \mathcal{H}_2; \tag{5.4}$$

$$\text{(2)}\quad \text{one asymptote of } \mathcal{H}_1 \text{ is parallel to } \mathcal{H}_2. \tag{5.5}$$

In figure 3, we sketch a standard rectangular hyperbola (we can always perform a transformation on one of the conics in (4.13) to the standard form) with centre (0, 0) (red curves), and another hyperbola satisfying the properties in (5.5). In figures 3(*a*,*b*), we see that $\mathcal{H}_1$ and $\mathcal{H}_2$ intersect at only one point, whilst in figures 3(*c*,*d*), we show how they can intersect at three points. In panel (*a*) we also see that the extra 'roots' predicted by Bézout's theorem are accounted for by the two curves 'intersecting' at infinity.

This analysis is important because naïvely solving (4.13) using a computer algebra package can be expensive and inefficient, and sometimes not even give an answer in the allotted time. In practice, it was found that the most computationally efficient method was to reduce (4.13) to a single cubic equation for B, say, and then apply the cubic formula to find the three roots in terms of a and b. Note that there is no way of knowing, *a priori*, that

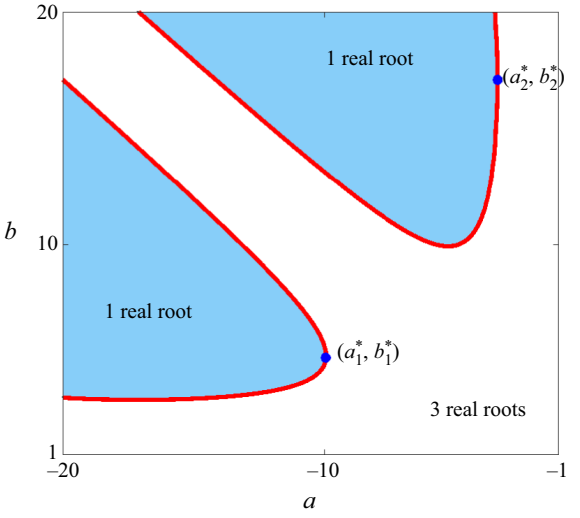

Figure 4. Regions in the (a, b) plane that result in one real root (shaded) or three real roots (non-shaded) for the staggered vortex configuration. The special parameter values (a_i^*, b_i^*), $i = 1, 2$ (as marked in the figure), correspond to transcritical bifurcations.

(4.13) reduces to a cubic equation. A double precision (a, b) mesh grid was constructed, and the roots calculated using the analytical expressions.

It should be noted that solutions to (4.13) are not necessarily valid solutions to the physical water-wave problem; this is because of the additional requirement that the mapping (4.1) is a one-to-one, or univalent, mapping from D to Ω. In the case of three pairs of real roots, the solution is non-unique for the given (a, b). However, as seen in the next subsection, a valid solution can only be constructed in certain regions of (a, b) parameter space. We can find the regions of (a, b) space where there are one or three roots by calculating the discriminant of the resulting cubic equation in terms of a and b. For inline vortices, i.e. when $ab > 0$, we find the discriminant is always positive except when $a = b$ and there is no solution, therefore there are always three real roots. For staggered vortices, $ab < 0$, the discriminant can be negative, allowing for a single real solution; figure 4 indicates these regions in the (a, b) plane. Before discussing these solutions in more detail, it is worth discussing the solution structure in two particular limits, when $a - b \to 0$ and when $a, b \to 1$.

5.1. *The limit $a - b \to 0$*

In this limit, applicable only to inline configurations, by multiplying both equations in (4.13) by $a - b$, and then taking the limit $a - b \to 0$, we find that (4.13) reduces to

$$\left.\begin{aligned} \hat{\lambda}_2 B^2 + \hat{\lambda}_3 AB + \hat{\lambda}_5 B = 0, \\ \hat{\mu}_1 A^2 + \hat{\mu}_3 AB + \hat{\mu}_4 A = 0, \end{aligned}\right\} \tag{5.6}$$

where $\hat{\lambda}_i = (a - b)\lambda_i$, $\hat{\mu}_i = (a - b)\mu_i$. This has a single trivial solution $(A, B) = (0, 0)$; the other roots do not exist as $\hat{\lambda}_2\hat{\mu}_3 - \hat{\lambda}_3\hat{\mu}_1 = 0$. Physically, this limit corresponds to a flat profile with two increasingly close vortices that effectively disappear when $a = b$.

5.2. *The limit $a, b \to -1$*

In this limit (concentrating on $a \to -1$, as the limit $b \to -1$ is similar), if we multiply the terms in (4.13) by $(a^2-1)^2$ and take the limit as $a \to -1$, then we find that all of the coefficients vanish identically. However, the dominant behaviour of (4.13) in this limit is

$$\bar{\lambda}_4 A \sim 0, \quad \bar{\mu}_5 B \sim 0, \tag{5.7a,b}$$

where $\bar{\lambda}_i = (1-a^2)^2\lambda_i$ and $\bar{\mu}_i = (1-b^2)^2\mu_i$. Therefore, as $a, b \to -1$, $(A, B) \to 0$.

6. Characterization of the equilibria

The inline and staggered configurations will be considered separately. In each case, the solution space for (A, B) is discussed as functions of the free parameters (a, b). In what follows, a valid solution is defined to be a set of parameters (a, b) with solutions (A, B) of (4.13) for which the mapping in (4.1) is univalent, i.e. there are no intersections of the interface in the physical z plane. We will discuss the conditions of validity as they arise in the analysis. Finally, we note that all of the numbered solution profiles in the subsequent discussion can be reproduced using the data provided in Appendix B, and that a simple exemplar code can be found at https://doi.org/10.6084/m9.figshare.22128548.v3.

6.1. *The inline (unstaggered) vortex street*

As mentioned in the previous section, inline vortices ($ab > 0$) have a positive discriminant of (4.13), and there are always three pairs of real solutions. Figures 5(*a*,*b*) show the solutions A and B, respectively, as b is varied when $a = -2$. Each different coloured branch represents one of the roots of (4.13), with solid/dotted lines indicating univalent/non-univalent mappings. For $a = -2$, there is only a small portion of one branch that contains univalent mappings and thus represent physical wave profiles. The limiting profiles (1 and 3) that occur at the ends of this branch portion both self-intersect with a neighbouring period window when $\zeta \neq 1$. The profile labelled 2 indicates a solution that is almost flat in the far field. We remark that the solution branch crosses the line $a = b$, but no solution exists when $a = b$ exactly. When $b < a$, the z_a vortex is the upper vortex, and vice versa when $b > a$.

The vortex strengths Γ_a and Γ_b are plotted in the inset diagrams of figures 5(*a*,*b*), respectively. The circulations at the limiting profile, labelled 3, are $\Gamma_a = 0.2711$, $\Gamma_b = -30.5539$, which indicates that the lower z_a vortex has significantly less influence on the flow than the upper z_b vortex. The circulations of the other limiting profile, labelled 1, are $\Gamma_a = -30.4596$, $\Gamma_b = 3.8487$, so that although the lower z_b vortex has less influence on the flow than the upper z_b vortex, it is not as weak as the lower vortex in profile 3.

For different values of a, we can vary b and larger portions of the solution branch result in valid mappings. We emphasize that in each case, only one root branch results in valid univalent solutions. Figure 6 shows the valid branch for values $a = -14, -7$ and -2. As can be seen in figure 6(*a*), the $a = -14, -7$ solution branches have a longer range of validity as $b \to -\infty$, but terminate at a lower value on the right-hand side of the curve. In each case, the limiting profiles, i.e. profiles 6 and 9 (and profile 3 in figure 5) self-intersect with an adjacent period window. As $b \to \infty$, a solution persists for $a = -14, -7$, corresponding to an elevation profile. As $b \to a$, $A, B \to 0$ (see § 5.1) and the profile becomes flat, as shown in profile 8 when $a = -14$, $b = -14.334$. This is because $A = B = 0$, and hence $\Gamma_a + \Gamma_b = 0$ as shown in figure 7.

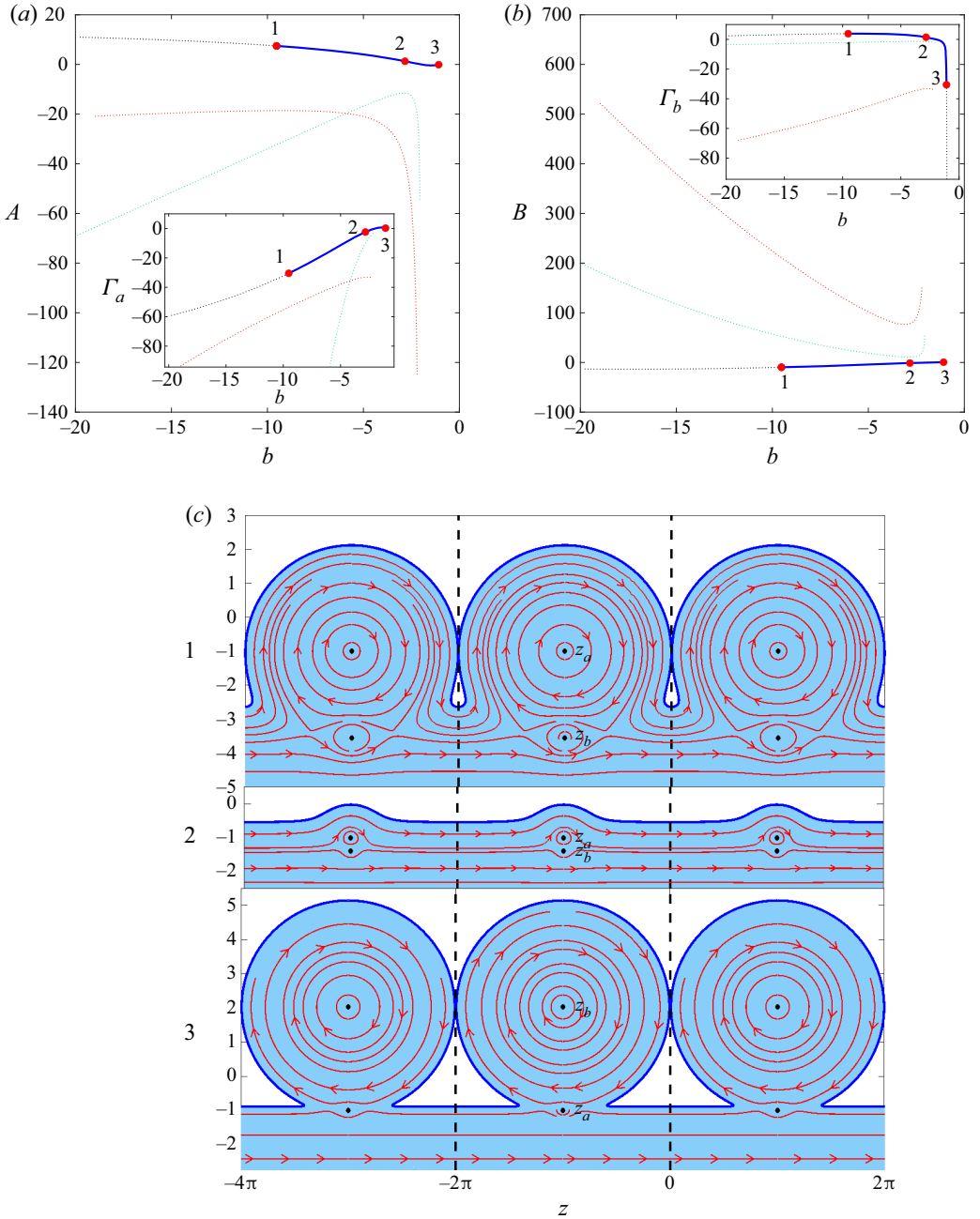

Figure 5. Solution structure for inline vortices with $a = -2$. (a,b) Plots of A, B, respectively, as b is varied. The inset diagrams show the variations of the vortex strengths, Γ_a and Γ_b, respectively. The solid lines indicate solutions of (4.13) that result in a univalent mapping. Thin dotted lines indicate solutions of (4.13) that do not result in a valid solution. (c) The streamlines and profiles are shown for the solutions labelled 1, 2 and 3, as well as the positions of the vortices.

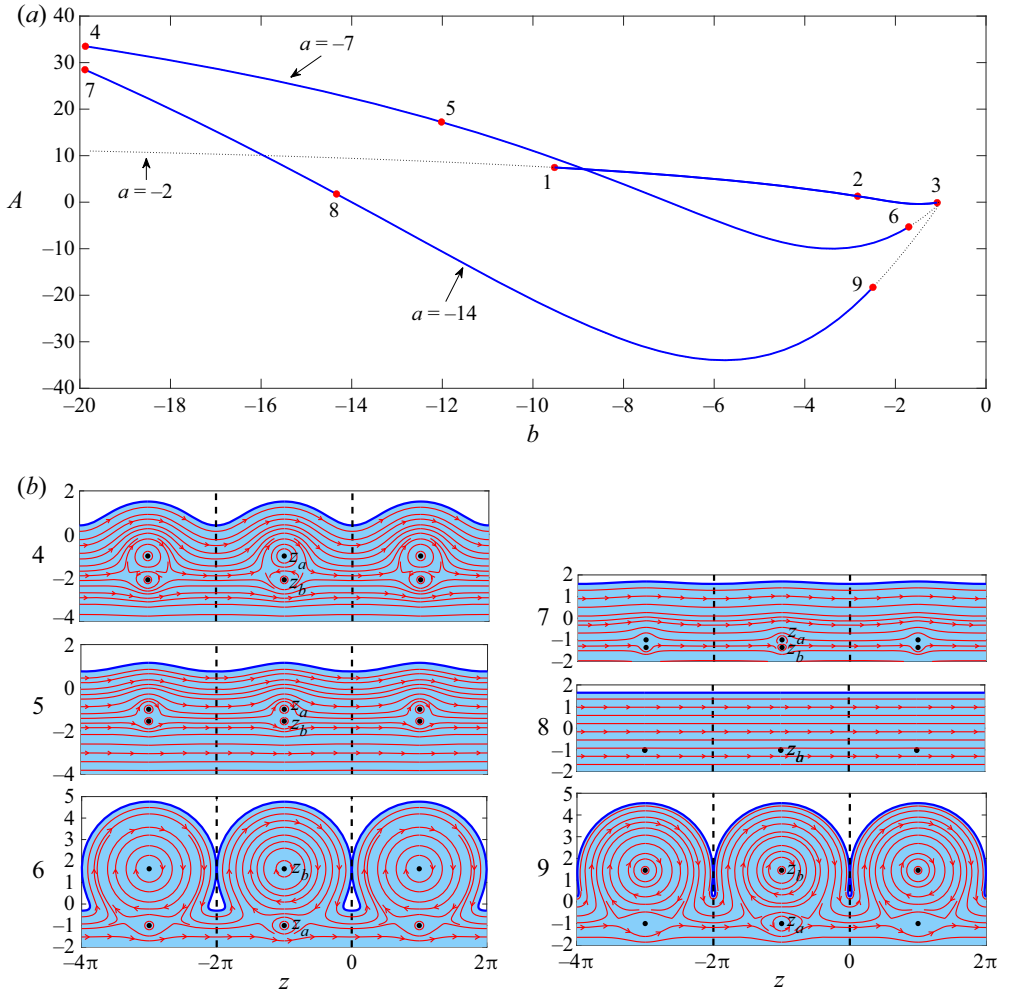

Figure 6. Solution structure for inline vortices, $a = -14, -7, -2$. (*a*) Plot of A as b is varied. The solid lines indicate solutions of (4.13) that result in a univalent mapping. Thin dotted lines indicate solutions of (4.13) that do not result in valid solutions. (*b*) The numbered profiles correspond to the labelled dots in the (b, A) solution space in (*a*).

Exploring the solution space further, as $b \to 1$, it is found that the curves all collapse to $(A, B) = (0, 0)$ as discussed in § 5.2. However, this limit will depend on the value of a, as demonstrated in figure 8. Here, we show how the range of valid solutions in b shrinks as $a \to -1$. The lower limit occurs at larger values of b (profiles in figure 8*a*) and the upper limit appears to increase towards $b = -1$ (profiles in figure 8*c*). The heights of the upper limit profiles do not change monotonically as a increases towards -1, so although it appears that the curves are converging on the same solution, they converge only in the limit as both $a, b \to -1$.

The limiting profiles are qualitatively different to those of Crowdy & Nelson (2010). For a single vortex, a cusp would appear in the middle of the period window for a critical value of a, beyond which a univalent mapping is not possible. This feature is not observed here. Instead, a profile intersects with that in an adjacent period window.

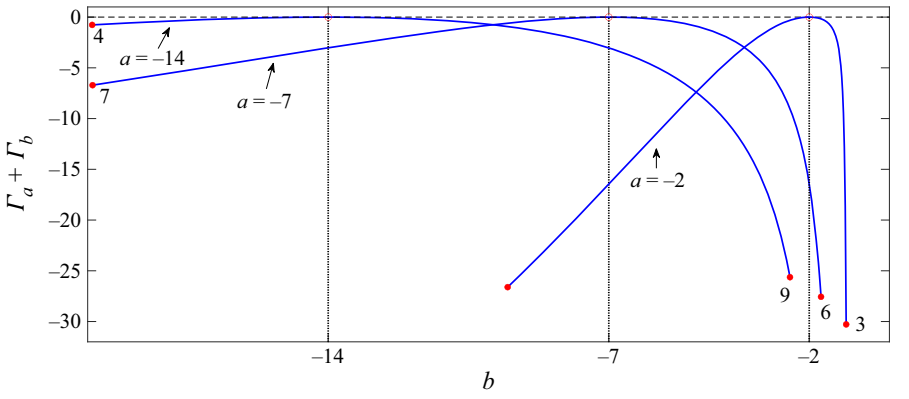

Figure 7. Total circulation of inline vortices, $a = -14, -7, -2$. The labels and solid dots indicate solutions in figure 6. The vertical dotted lines indicate where $a = b$ on each branch, and the hollow dots indicate where there is no solution. The dashed horizontal line indicates $\Gamma_a + \Gamma_b = 0$.

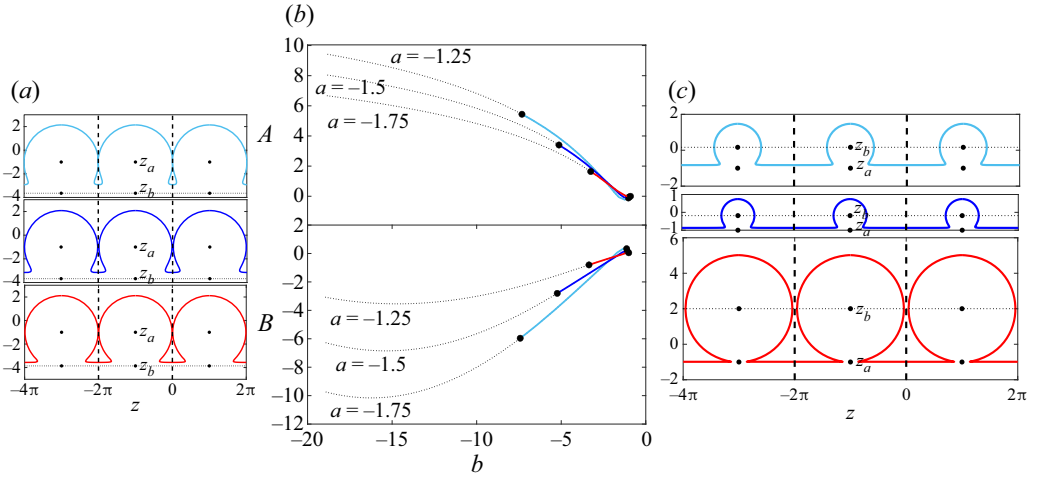

Figure 8. Solution structure of inline vortices, $a = -1.75, -1.5, -1.25$. (*a*) The profiles correspond to the markers furthest to the left in (*b*). (*b*) The top plot shows A, and the bottom plot shows B, as b is varied. The solid lines indicate solutions of (4.13) that give a univalent mapping. Thin dotted lines indicate solutions of (4.13) that do not result in valid solutions. (*c*) The profiles correspond to the marker furthest to the right in (*b*).

6.2. *The staggered vortex street*

Staggered vortices require that $ab < 0$. As shown in figure 4, there are regions in (a, b) space that result in a unique solution. This is explored further by examining the solution space for a fixed value of a and then varying b, as done previously for the inline case.

Figures 9(*a*,*b*) show the values of A and B, respectively, when $a = -7$. For sufficiently large b, there is only one single root of (4.13) that does not represent a valid solution. At $b \approx 10.68$, two additional solution branches appear via a fold bifurcation, both corresponding to valid solutions, as seen in the profiles labelled 1, 2 and 3. The lower branch is a valid solution only until the profile develops a cusp in the middle of the period window, as seen in the profile labelled 1. This is similar to the limiting profiles in Crowdy & Nelson (2010), and occurs at parameter values (a, b) such that $z'(1) = 0$.

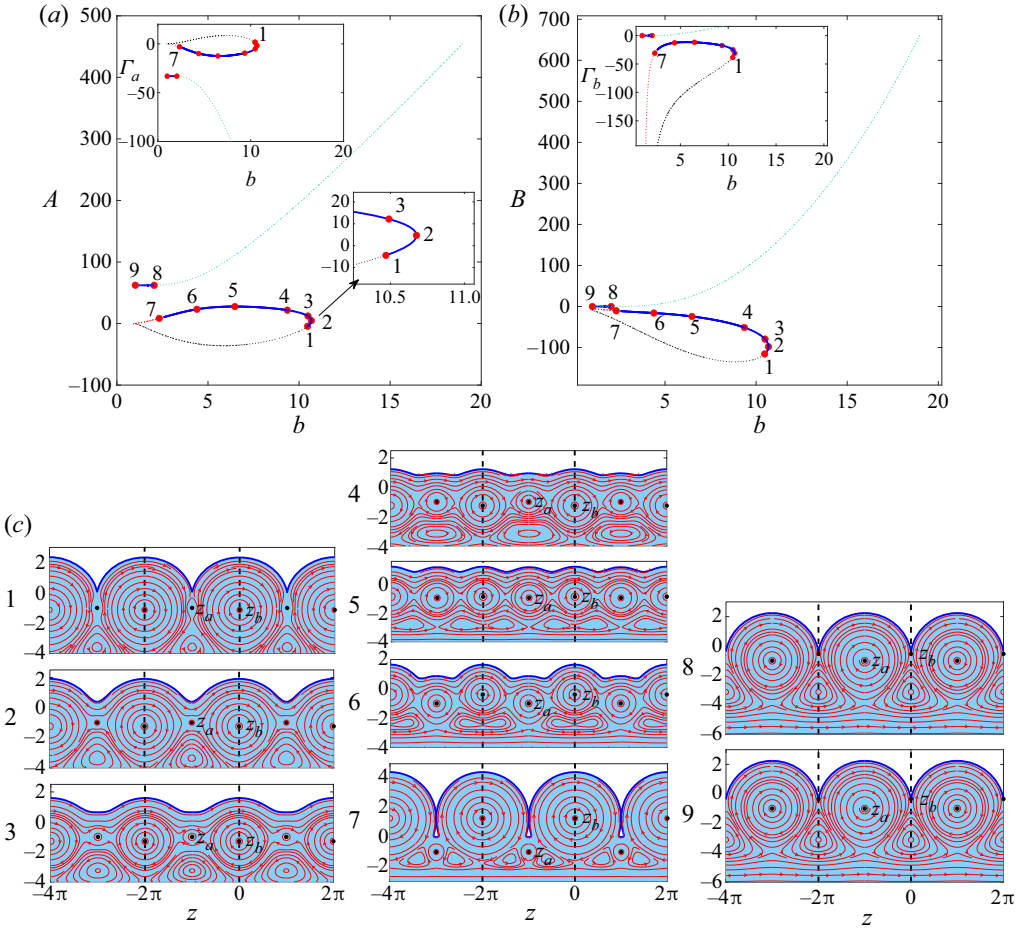

Figure 9. Solution structure for staggered vortices, $a = -7$. (a,b) Plots of A, B, respectively, as b is varied. The inset diagrams show the variations of the vortex strengths, Γ_a and Γ_b, respectively. The solid lines indicate solutions of (4.13) that result in a univalent mapping. Thin dotted lines indicate solutions of (4.13) that do not result in a valid solution. (c) The streamlines and profiles are shown for the solutions labelled 1–9.

Continuing on the upper branch as b decreases, the profiles become bimodal, with two distinct profile peaks (see profile 4) until $b = -a$, which corresponds to two horizontally aligned vortices (as seen in profile 5) where the profile is unimodal. Decreasing b further results in more distinct bimodal wave profiles (see profile 6) until the branch reaches a termination point at $b \approx 2.3235$, when the interface self-intersects with an adjacent period window (see profile 7).

Interestingly, for values of b less than this value, there is a small portion of the other branch that allows valid solutions (see profiles 8 and 9). These profiles are similar in that both have a cusp at the edge of the period window, corresponding to $Z'(-1) = 0$. In profile 9, z_b is close to the cusp, which is as expected as $b \to 1$; however, as seen in the inset of figure 9(b), the strength of the vortex at z_b in this limit is zero, rendering this vortex harmless.

This bifurcation structure for $a = -7$ is not generic as a is varied. Figures 10(a–c) show the structure for $a = -14, -7, -2$, respectively. When $a = -14$, there are always three

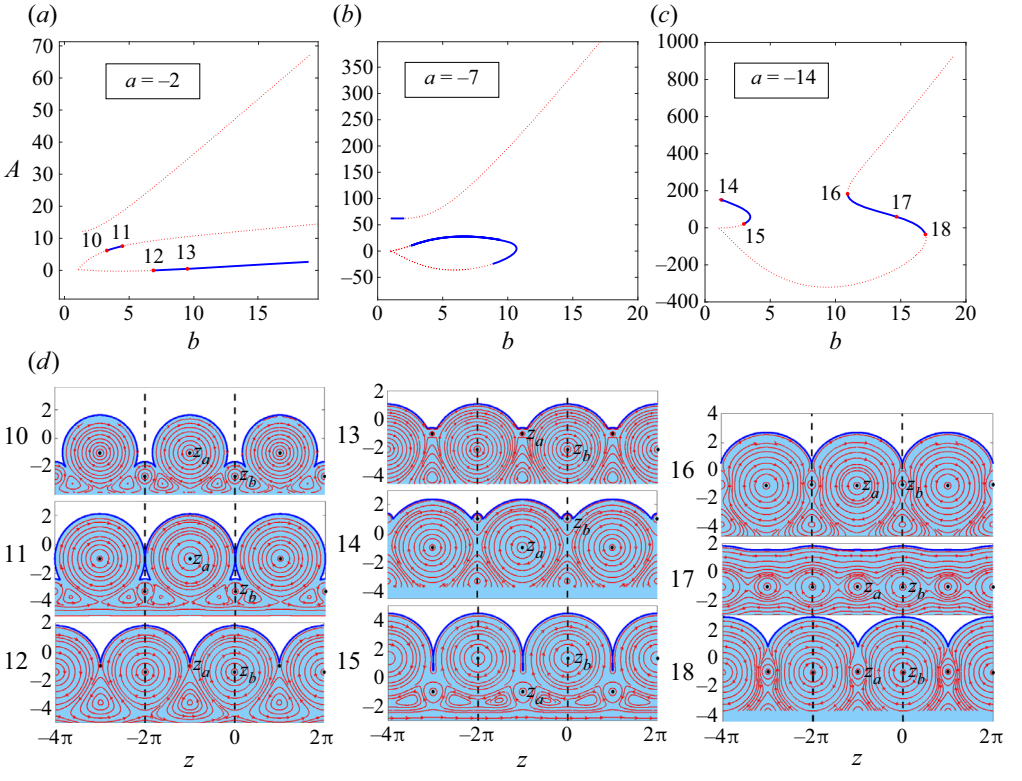

Figure 10. Solution structure for staggered vortices: (*a*) $a = -14$, (*b*) $a = -7$, and (*c*) $a = -2$. The solid lines indicate solutions of (4.13) that result in a univalent mapping. Thin dotted lines indicate solutions of (4.13) that do not result in a valid solution. (*d*) The streamlines and profiles are shown for the solutions labelled 10–18.

roots and the fold bifurcation present when $a = -7$ ceases to exist. The profiles on the portions of the branches that are physically admissible are significantly different to the $a = -7$ case.

The 'upper' branch in figure 10(*a*) has no physically admissible solutions, and the 'middle' branch terminates on the 'left' when the profile develops a cusp close to the edge of the period window (see profile 10) and terminates on the 'right' when the interface intersects with the profile in an adjacent period window. The 'lower' branch, as b increases from 1, starts to produce a physically admissible solution when a cusp develops in the middle of the period window (see profile 12) and for the parameter values that we sampled, continue to provide a physically admissible solution as b increases, resulting in a bimodal wave profile, as seen in profile 13.

The structure changes again when a becomes smaller, as shown in figure 10(*c*), when $a = -2$. The different roots interact in a non-trivial manner through a number of different fold bifurcations. Starting at small $b > 1$, profile 14 shows that the 'upper' branch starts when there is a cusp near the edge of the period window, continues through a fold, and eventually terminates when the profile self-intersects (see profile 15). There is a large region of b values that does not produce a physically admissible solution until a cusp develops at the edge of the window (see profile 16), and then there is a single branch of solutions, eventually terminating when a cusp develops at the middle of the period

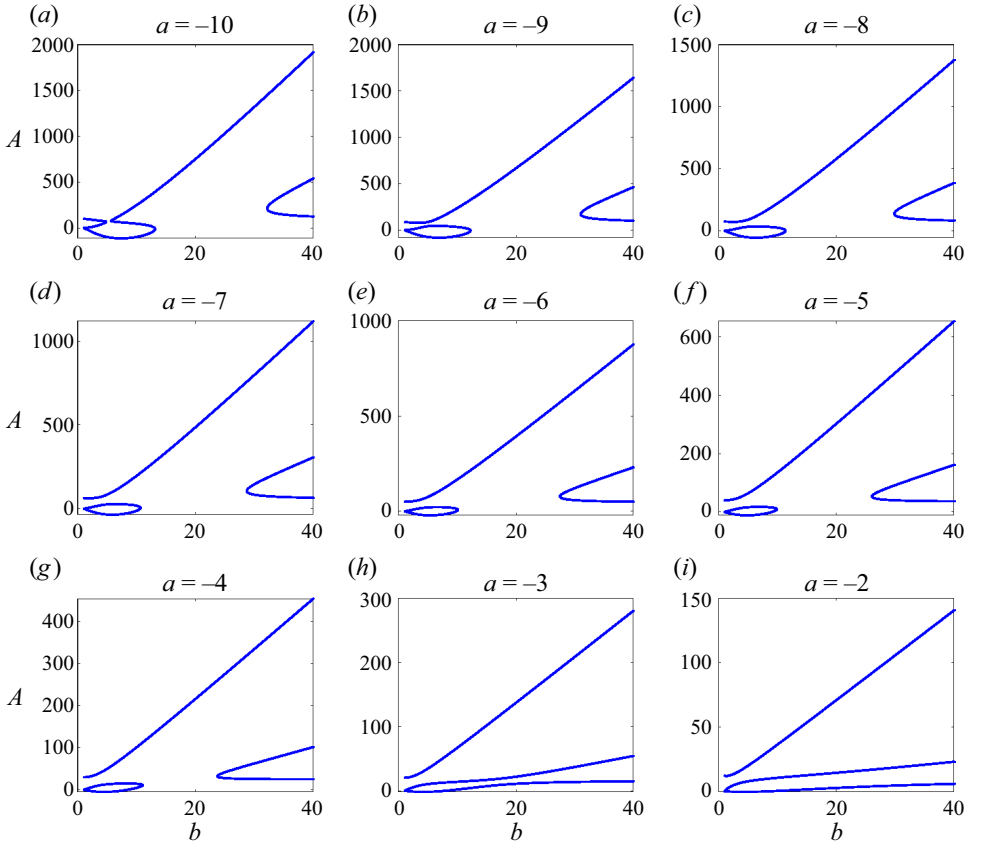

Figure 11. Solution structure for staggered vortices as a varies from -10 to -2. Each plot is of A versus b, with the value of a as shown. The roots are shown regardless of whether or not they represent valid physical mappings.

window (see profile 18). Interestingly, these termination points appear to coincide close to fold bifurcations.

The structure of the equilibria for the staggered vortex system is clearly rich and intriguing. Because the discriminant of (4.13) can change sign, the number of real solutions varies, which results in a non-trivial interaction of the solution branches. This results in quite exotic profiles, containing cusps and self-intersections. These do not have direct counterparts in the case of a single cotravelling vortex row (Crowdy & Nelson 2010).

Exploring this further, the parameter a can be varied to identify two transcritical bifurcations in the solution space. These occur when the two fold bifurcations collide, and are shown in figure 4 as (a_i^*, b_i^*). Figure 11 shows how the (b, A) bifurcation diagram evolves as a increases from -10 to -2. The first transcritical bifurcation occurs when the 'hook' structure at small b self-intersects and becomes a closed loop; see $a = -10$ and $a = -9$. The first bifurcation occurs at $a_1^* = -9.9336$ to 4 d.p. The second transcritical bifurcation occurs when the 'loop' structure intersects the lower branches for large b; see $a = -4$ and $a = -3$. This second bifurcation occurs at $a_2^* = -3.3575$ to 4 d.p. The bifurcation diagram for $a = a_1^*$ is shown in figure 12, where we identify sections of the curve that result in valid mappings (solid blue lines). The limiting profiles are indicated by the labels. Particular attention is drawn to profile 19, which has a small unusual circular

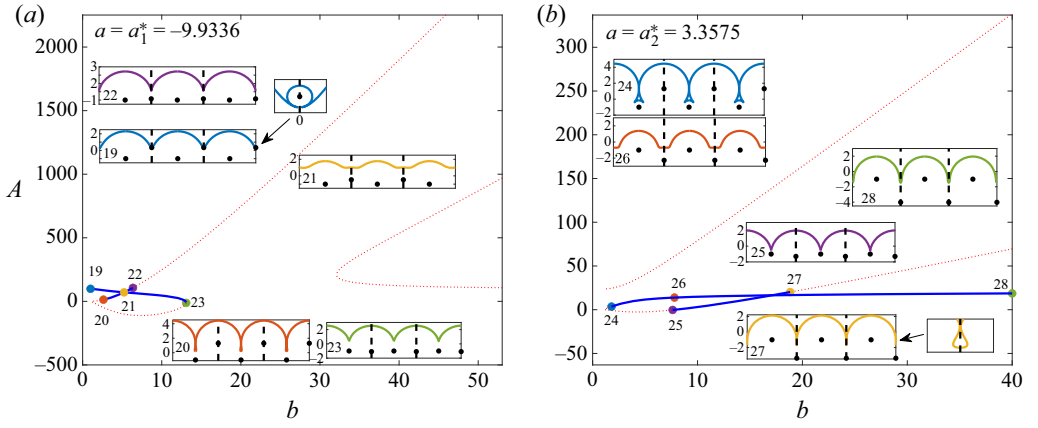

Figure 12. Solution structure for $a = a_1^*, a_2^*$. (*a*,*b*) Plots of A as b is varied, for $a = a_1^*, a_2^*$, respectively. The solid blue lines represent valid physical solutions. Limiting profiles are marked with labels.

cusp at the edge of the periodic window. Finally, no further bifurcations are observed as a decreases from -14; the bifurcation structure remains robust as $a \to -\infty$.

6.3. *The limit* $|a|, |b| \to \infty$

The limiting case where $|a|, |b| \to \infty$ is of significant interest. In this limit, the free surface is expected to recede from the vortex rows into large positive y values and become increasingly flat as deformation effects from the vortices weaken. It might be anticipated that the limiting equilibria would be von Kármán vortex streets in unbounded shear; but it was established in § 3 that no such equilibria exist.

Consider the case of staggered vortices with $b = -a$ and $a > 0$, and let $a \to \infty$. From the explicit expressions given in Appendix A, it can be shown that

$$\lambda_2, \lambda_3 \sim O(1/a), \quad \lambda_4 \sim 4\log a - a^2, \quad \lambda_5 \sim 4\log a + a^2, \quad \lambda_6 = -4a^3 \log a, \tag{6.1a–d}$$

so that the first equation of (4.10) becomes

$$(4\log a - a^2)A + (4\log a + a^2)B - 4a^3 \log a \sim 0. \tag{6.2}$$

From a similar analysis, the second equation of (4.10) becomes

$$(4\log a + a^2)A + (4\log a - a^2)B + 4a^3 \log a \sim 0. \tag{6.3}$$

Together, these two equations imply that

$$A = -B \sim -2a\log a. \tag{6.4}$$

Consequently, as $a \to \infty$,

$$z = Z(\zeta) \sim \mathrm{i}\left[\log\zeta - \frac{2a\log a}{\zeta - a} + \frac{2a\log a}{\zeta + a}\right] + d \sim \mathrm{i}[\log\zeta + 4\log a] + d. \tag{6.5}$$

The condition $z_a = Z(1/a) = -\mathrm{i}$ then implies

$$-\mathrm{i} = Z(1/a) = \mathrm{i}\left[\log(1/a) + \frac{Aa}{1 - a^2} + \frac{Ba}{1 - ab}\right] + d, \tag{6.6}$$

implying that

$$d \sim -\mathrm{i}(1 + 3\log a). \tag{6.7}$$

It follows from (6.5) that

$$Z(\zeta) \sim \mathrm{i}[\log\zeta + 4\log a] + d = \mathrm{i}[\log\zeta + 4\log a - (1 + 3\log a)] = \mathrm{i}\log(\zeta a) - \mathrm{i}. \tag{6.8}$$

Suppose also that we insist that $z_b = Z(1/b) = \pi - \mathrm{i}(1 + \lambda)$. Then

$$\mathrm{i}\left[\log(1/b) + \frac{Ab}{1-ab} + \frac{Bb}{1-b^2} - 1 - \log(1/a) - \frac{Aa}{1-a^2} - \frac{Ba}{1-ab}\right] = \pi - \mathrm{i}(1+\lambda). \tag{6.9}$$

On use of (6.4), it follows from this that $\lambda \to 0$, so the two vortices per period tend to $y = -1$ and are separated by distance π. From (4.9) and (4.10),

$$-\frac{\mathrm{i}\Gamma_a}{2\pi} = -\frac{A\,Z'(1/a)}{2a^2} \sim -\frac{\mathrm{i}A}{2a}, \quad -\frac{\mathrm{i}\Gamma_b}{2\pi} = -\frac{B\,Z'(1/b)}{2b^2} \sim -\frac{\mathrm{i}B}{2b}, \tag{6.10a,b}$$

where we have used the fact that as $a \to \infty$, $Z(\zeta) \sim \mathrm{i}\log\zeta + \text{const.}$. But this means that

$$\Gamma_a \sim \Gamma_b = -2\pi\log a. \tag{6.11}$$

The limiting configuration is not therefore the degenerate staggered von Kármán vortex street in unbounded shear found in § 3. Rather, it is a single vortex row, with period π, of identical point vortices with circulation Γ_a. It therefore falls within the class of solutions considered by Crowdy & Nelson (2010); indeed, it is easy to verify that (6.4) is consistent with (22) of Crowdy & Nelson (2010) as an analogous parameter $a \to \infty$ in that study. The new staggered equilibria found here can therefore be viewed as a steady 'pairing mode' bifurcation from the latter solutions, that is, a class of subharmonic bifurcations wherein adjacent pairs of vortices in a period-π equilibrium found by Crowdy & Nelson (2010) displace separately to destroy the original periodicity forming instead one of the 2π-periodic generalized equilibria found here.

An analysis of the inline case follows similarly. In this case, for $b \approx a \to \infty$, the limiting configuration is found to be an inline, or symmetric, von Kármán vortex street of vanishing aspect ratio $\lambda \to 0$ corresponding to the situation where the two vortex rows sit on top of each other and eventually cancel each other out.

The significance of all these observations is that while the results of § 3 show that non-trivial equilibria generalizing the classical von Kármán vortex streets do not exist in unbounded linear shear flow, a rich array of steadily travelling equilibria exists when a cotravelling free surface is also present.

7. Discussion

There has been much recent interest in the problem of water waves with vorticity (Haziot *et al.* 2022), and analytical solutions are rare. This paper has unveiled a novel two-parameter family of analytical solutions for steadily travelling water waves with uniform vorticity and superposed von Kármán point vortex streets. These solutions are direct extensions of earlier work on water waves with uniform vorticity and single cotravelling vortex row found by Crowdy & Nelson (2010). All these solutions fall within 'case 1' of a three-case categorization of water waves with vorticity set out recently by Crowdy (2022).

Fundamental to constructing the equilibria is finding the solution of a pair of algebraic nonlinear equations, which in the case of two vortices per period, has either one or three

real roots that can be written and calculated in exact analytical form. The solution space for inline configurations is simpler in that there are always three real roots, but only one root branch results in a univalent conformal map. These solution branches terminate when the wave profile intersects with that in an adjacent period window. For staggered configurations, the solution space is more complicated as there are regions of parameter space where only a single real root exists. For these configurations, limiting profiles can exist where cusps form, or where the interface intersects, resulting in a rich variety of solutions, including bimodal wave profiles and fold bifurcations.

The stability of the various equilibria found here is clearly of great interest, but requires detailed investigation and has not been studied here. Crowdy & Cloke (2002) have studied the linear stability of analogous case 1 solutions in the radial (vortex) geometry, and found that exact solutions within this class can be linearly stable. The methods used in that study are easily adaptable to study the stability of the new water wave equilibria found here. More recently, Blyth & Părău (2022) have calculated the exact linear stability spectrum of the waves described in Hur & Wheeler (2020) – which fit into case 3 of the taxonomy of Crowdy (2022) – and those methods should also be generalizable to the solutions presented here.

The method that we describe here can easily be extended to n submerged point vortex rows. For n vortices per period there will arise an n-parameter family of solutions with a system of n quadratic relations to be solved. From Bézout's theorem, this means that there will be potentially 2^n possible solutions; the complexity of the solution space increases exponentially as n increases. For $n = 3$, the equations are easy to solve using a symbolic algebra package, but the complexity of the closed-form solution means that because of the computer time taken to solve the system symbolically, and then convert to double precision numbers, it is inefficient to calculate the roots in this way. For example, choosing $(a, b, c) = (-2, -3, -4)$, where c represents the parameter of the third vortex, takes approximately 200 computer seconds to compute the roots symbolically and then convert to a double precision number. Interestingly, by an extension of the degeneracies evident here, and in the earlier study of Crowdy & Nelson (2010), five roots are obtained, rather than the eight predicted. So far, after limited investigation, we have observed that none of these roots results in a valid univalent map. However, we leave the existence of steady n-vortex configurations as an open question.

More broadly, it is worth mentioning that other extensions of the classical von Kármán point vortex streets have been found. Crowdy & Green (2011) have found analytical solutions for steadily travelling streets of so-called hollow vortices that are finite-area regions of constant pressure having non-zero circulation around them. These solutions can be understood as regularized von Kármán vortex streets where the singular point vortices are replaced by finite-area vortices for which the associated velocity fields are everywhere finite. This hollow vortex model has much in common with the water wave problem in that the boundary condition on the boundary of a hollow vortex, which also neighbours a constant-pressure region, is akin to that on the free surface between a water wave and a constant-pressure region. Crowdy & Roenby (2014) discuss the similarities between these two problems. In view of the new equilibrium solutions found here, and the new case 2 solutions for submerged von Kármán point vortex streets beneath a free surface found recently in Crowdy (2022), it is of interest to examine if the hollow vortex street equilibria of Crowdy & Green (2011) can be generalized to incorporate steady translation beneath a cotravelling free surface wave in the spirit of the present study. Such matters await further investigation.

The effects of gravity and surface tension have been ignored but how they will alter the new wave solutions found here is clearly of interest. It might be argued that the richness of the solution structure found here, even without gravity or surface tension effects, underlines the theoretical importance of understanding this case first before adding in other physical effects. It should be possible to add the effect of weak gravity as a regular perturbation, an analysis that should be facilitated greatly by having available closed-form expressions for the leading-order equilibria. Such analyses have recently been carried out for constant-vorticity leading-order solutions by Hur & Wheeler (2021); see also Akers, Ambrose & Wright (2013), who added weak gravity to irrotational capillary waves. Asymptotic analyses of the effects of weak capillarity (Chapman & Vanden-Broeck 2002) on the solutions here will similarly be made easier by the closed-form description of the equilibria.

Finally, we would like to discuss the broad importance of these solutions and the framework established in Crowdy (2022) in the general context of the water wave problem. Whilst existence theorems for the water wave problem exist for different physical effects and geometries (see e.g. Haziot *et al.* 2022), they are usually not constructive, and typically researchers have to rely on model equations (e.g. in the case of gravity waves in finite depth, the Korteweg–de Vries equation; for others, see Lannes 2013), asymptotic analysis (see e.g. Chapman & Vanden-Broeck 2002) and/or numerical methods. The solutions here and in Crowdy (2022) are therefore of special importance as they can: (i) provide a validation for any numerical code; (ii) provide a leading-order term in a perturbation expansion for small gravity (i.e. the large Froude number limit) or small surface tension; and, perhaps most importantly, (iii) do not require sophisticated mathematical techniques to find and visualize them; the solution of a set of algebraic nonlinear equations and a few lines of MATLAB code are all that is required. It is the hope, and indeed aim, that these solutions can act as a springboard to solutions in other physical settings, and there is realistic potential for other more exact solutions to be found. To quote Whitham (1974) in the last sentence of his seminal work on water waves: 'Not least is the lesson that exact solutions are still around and one should not always turn too quickly to a search for ε'.

Acknowledgements. This work was developed as a result of a series of invited summer school lectures delivered by D.G.C. at the LMS-Bath 'New Directions in Water Waves Workshop and Summer School' held at the University of Bath in July 2022. Both authors attended this event and are grateful to the LMS and the organizers (P. Milewski, M. Wheeler, P. Trinh and V. Hur) for facilitating it.

Funding. J.S.K. acknowledges funding from the Leverhulme Trust, ECF-2021-017.

Declaration of interests. The authors report no conflict of interest.

Data availability statement. The code that supports the findings of this study is openly available at https://doi.org/10.6084/m9.figshare.22128548.v3.

Author ORCIDs.
Jack S. Keeler https://orcid.org/0000-0002-8653-7970;
Darren G. Crowdy https://orcid.org/0000-0002-7162-0181.

Author contributions. Both authors contributed to developing the theory and results in this paper. All numerical calculations were performed by J.S.K.

I	Profile	a	b	A_1	A_2	A_3	B_1	B_2	B_3
	1	−2	−9.5233	**7.4617**	−32.2907	−18.5781	**−9.6685**	52.4604	210.9486
	2	−2	−2.8335	**1.2889**	−11.5388	−39.2653	**−1.2143**	10.9391	78.2877
	3	−2	−1.0784	**−0.1003**	0.1355	14.5455	**0.49719**	−0.6703	−0.9163
	4	−7	−19.8778	**33.5114**	−989.9282	−1025.0357	**−58.7433**	2120.7896	3675.6522
	5	−7	−12.0187	**17.2380**	−914.9454	−1301.6490	**−22.9983**	1313.8903	2585.6846
	6	−7	−1.7057	**−5.3123**	115.9642	19.8468	**5.0539**	−10.2229	−16.5033
	7	−14	−19.8874	**28.4763**	−9663.6168	−12825.9029	**−35.6378**	12803.6777	19352.3998
	8	−14	−14.3354	**1.7648**	−95176.5334	−143764.8402	**−1.7910**	96932.0286	147888.7231
	9	−14	−2.4963	**−18.2925**	470.6813	171.3329	**11.7264**	−41.1664	−75.0930
S	Profile	a	b	A_1	A_2	A_3	B_1	B_2	B_3
	1	−7	10.4692	12.5422	**−4.4173**	208.3766	−78.5103	**−115.6944**	130.3844
	2	−7	10.6757	4.8517	**4.5931**	213.9207	−97.3818	**−97.9591**	138.2260
	3	−7	10.4898	**12.1763**	−3.9217	208.9281	**−79.4839**	−114.8426	131.1558
	4	−7	9.3546	**21.7266**	179.1019	−19.9683	**−51.1867**	92.2319	−133.7416
	5	−7	6.4737	**27.5964**	110.9992	−35.5523	**−24.2027**	25.5053	−115.1951
	6	−7	4.3895	75.6490	**23.1642**	−32.8419	4.4199	**−15.9276**	−77.1505
	7	−7	2.3225	62.4804	**8.4013**	−16.1444	0.0424	**−10.4572**	−32.7988
	8	−7	2.0437	**62.1484**	6.2842	−12.7962	**−0.0050**	−9.4768	−27.1818
	9	−7	1.0105	**62.1883**	0.04689	−0.1034	**0.0000**	−5.2346	−9.2915

Table 1. Table of values of a and b, with solutions A and B. The bold values are the values that produce the profiles, whilst the other roots are also listed for completeness. The inline values (I) correspond to profiles in figures 5 and 6, whilst the staggered values (S) correspond to the profiles in figure 9. Values reported to 4 d.p.

Appendix A. Coefficients of (4.13) for A and B

The coefficients of (4.13) are found to be

$$\left.\begin{aligned} \lambda_1 = 0, \quad \lambda_2 = \frac{2a^4(a^2-1)}{(a-b)(ab-1)^3}, \quad \lambda_3 = \frac{2a^4(b^2-1)}{(a-b)(ab-1)^3}, \\ \lambda_4 = \frac{a^2(2a^2\log(a^2) - a^4 + 1)}{(a^2-1)^2}, \\ \lambda_5 = \frac{2a^3(ab + a^2\log(a^2) - a^3b + a^2 - ab\log(a^2) - 1)}{(a-b)(ab-1)^2}, \\ \lambda_6 = -2a^3\log(a^2) \end{aligned}\right\} \tag{A1}$$

and

$$\left.\begin{aligned} \mu_2 = \frac{2b^4(b^2-1)}{(b-a)(ab-1)^3}, \quad \mu_2 = 0, \quad \mu_3 = \frac{2b^4(a^2-1)}{(b-a)(ab-1)^3}, \\ \mu_4 = \frac{2b^3(ab + b^2\log(b^2) - b^3a + b^2 - ab\log(b^2) - 1)}{(b-a)(ab-1)^2}, \\ \mu_5 = \frac{b^2(2b^2\log(b^2) - b^4 + 1)}{(b^2-1)^2}, \quad \mu_6 = -2b^3\log(b^2). \end{aligned}\right\} \tag{A2}$$

Appendix B. Values of parameters

In table 1, we list the values of a and b, together with their solutions A and B for reproducibility purposes, for a selection of the numbered profiles in this paper. These can also be reproduced by the MATLAB script found at https://doi.org/10.6084/m9.figshare.22128548.v3.

References

ACHESON, D.J. 1990 *Elementary Fluid Dynamics*. Oxford University Press.

AKERS, B.F., AMBROSE, D.M. & WRIGHT, J.D. 2013 Gravity perturbed Crapper waves. *Proc. R. Soc. Lond.* A **470**, 20130526.

BENJAMIN, T.B. 1962 The solitary wave on a stream with an arbitrary distribution of vorticity. *J. Fluid Mech.* **12**, 97–116.

BÉZOUT, E. 1779 Théorie générale des équations algébrique. De l'imprimerie de PhD Pierres.

BLYTH, M.G. & PĂRĂU, E.I. 2022 Stability of waves on fluid of infinite depth with constant vorticity. *J. Fluid. Mech.* **936**, A46.

CHAPMAN, S.J. & VANDEN-BROECK, J.-M. 2002 Exponential asymptotics and capillary waves. *SIAM J. Appl. Maths* **62**, 1872–1898.

CONSTANTIN, A. & STRAUSS, W. 2004 Exact steady periodic water waves with vorticity. *Commun. Pure Appl. Maths* **57**, 481–527.

CROWDY, D.G. 1999 A class of exact multipolar vortices. *Phys. Fluids* **11**, 2556–2564.

CROWDY, D.G. 2002*a* Exact solutions for rotating vortex arrays with finite-area cores. *J. Fluid Mech.* **469**, 209–235.

CROWDY, D.G. 2002*b* The construction of exact multipolar equilibria of the two-dimensional Euler equations. *Phys. Fluids* **14**, 257–267.

CROWDY, D.G. 2022 Exact solutions for steadily travelling water waves with submerged point vortices. *J. Fluid Mech.* **954**, A47

CROWDY, D.G. & CLOKE, M. 2002 Stability analysis of a class of two-dimensional multipolar vortex equilibria. *Phys. Fluids* **14**, 1862.

CROWDY, D.G. & GREEN, C.C. 2011 Analytical solutions for von Kármán streets of hollow vortices. *Phys. Fluids* **23**, 126602.

CROWDY, D.G. & MARSHALL, J.S. 2004 Growing vortex patches. *Phys. Fluids* **16**, 3122.

CROWDY, D.G. & MARSHALL, J.S. 2005 Analytical solutions for rotating vortex arrays involving multiple vortex patches. *J. Fluid Mech.* **523**, 307–338.

CROWDY, D. & NELSON, R. 2010 Steady interaction of a vortex street with a shear flow. *Phys. Fluids* **22**, 096601.

CROWDY, D.G. & ROENBY, J. 2014 Hollow vortices, capillary water waves and double quadrature domains. *Fluid Dyn. Res.* **46**, 031424.

DAVIS, P.J. 1974 *The Schwarz Function and its Applications*. American Mathematical Society.

EHRNSTRÖM, M. 2008 A new formulation of the water wave problem for Stokes waves of constant vorticity. *J. Math. Anal. Applics.* **339**, 4636–4643.

FILIPPOV, I. 1961 Motion of vortex beneath the free surface of a fluid. *Prikl. Mat. Mekh.* **25**, 242.

GROVES, M.D. & WAHLÉN, E. 2007 Spatial dynamics methods for solitary gravity–capillary water waves with an arbitrary distribution of vorticity. *SIAM J. Math. Anal.* **39**, 932–964.

GROVES, M.D. & WAHLÉN, E. 2008 Small-amplitude Stokes and solitary gravity water waves with an arbitrary distribution of vorticity. *Physica* D **237**, 1530–1538.

HAZIOT, S.V., HUR, V.M., STRAUSS, W.A., TOLAND, J.F., WAHLÉN, E., WALSH, S. & WHEELER, M.H. 2022 Traveling water waves – the ebb and flow of two centuries. *Q. Appl. Maths* **80**, 317–401.

HUR, V.M. & DYACHENKO, S.A. 2019*a* Stokes waves with constant vorticity: folds, gaps and fluid bubbles. *J. Fluid Mech.* **878**, 502–521.

HUR, V.M. & DYACHENKO, S.A. 2019*b* Stokes waves with constant vorticity: I. Numerical computation. *Stud. Appl. Maths* **142**, 162–189.

HUR, V.M. & VANDEN-BROECK, J.-M. 2020 A new application of Crapper's exact solution to waves in constant vorticity flows. *Eur. J. Mech. (*B*/Fluids)* **83**, 190–194.

HUR, V.M. & WHEELER, M.H. 2020 Exact free surfaces in constant vorticity flows. *J. Fluid Mech.* **896**, R1.

HUR, V.M. & WHEELER, M.H. 2022 Overhanging and touching waves in constant vorticity flows. *J. Diff. Equ*. **338**, 572–590.

LANNES, D. 2013 *The Water Waves Problem: Mathematical Analysis and Asymptotics*, vol. 188. American Mathematical Society.

LE, H. 2019 On the existence and instability of solitary water waves with a finite dipole. *SIAM J. Math. Anal.* **51**, 4074–4104.

PULLIN, D.I. & GRIMSHAW, R.H.J. 1988 Finite amplitude solitary waves at the interface between two homogeneous fluids. *Phys. Fluids* **31**, 3550–3559.

SAFFMAN, P.G. 1992 *Vortex Dynamics*. Cambridge University Press.

SHA, H. & VANDEN-BROECK, J.-M. 1995 Solitary waves on water of finite depth with a surface or bottom shear layer. *Phys. Fluids* **7**, 1048.

SHATAH, J., WALSH, S. & CHENG, C. 2013 Travelling water waves with compactly supported vorticity. *Nonlinearity* **26**, 1529–1564.

SIMMEN, J.A. & SAFFMAN, P.G. 1985 Steady deep water waves on a linear shear current. *Stud. Appl. Maths* **73**, 35–57.

TELES DA SILVA, A.F. & PEREGRINE, D.H. 1988 Steep, steady surface waves on water of finite depth with constant vorticity. *J. Fluid Mech.* **195**, 281–302.

TER-KRIKOROV, A.M. 1958 Exact solution of the problem of the motion of a vortex under the surface of a liquid. *Izv. Akad. Nauk. SSSR Ser. Mat.* **22**, 177–200.

TSAO, S. 1959 Behaviour of surface waves on a linearly varying current. *J. Geophys. Res*. **79**, 4498–4508.

VANDEN-BROECK, J.-M. 1994 Steep solitary waves in water of finite depth with constant vorticity. *J. Fluid Mech.* **274**, 339–348.

VANDEN-BROECK, J.-M. 1996 Periodic waves with constant vorticity in water of infinite depth. *IMA J. Appl. Maths* **56**, 207–217.

VARHOLM, K. 2016 Solitary gravity–capillary water waves with point vortices. *J. Discrete Continous Dyn. Syst.* **36**, 3927–3959.

WAHLÉN, E. 2009 Steady water waves with a critical layer. *J. Differ. Equ.* **246**, 2468–2483.

WHITHAM, G.B. 1974 *Linear and Nonlinear Waves*. John Wiley.